ACS Chemical Neuroscience

Research Article

pubs.acs.org/chemneuro

Thermodynamic Description of Beta Amyloid Formation Using Physicochemical Scales and Fractal Bioinformatic Scales

J. C. Phillips

Department of Physics and Astronomy, Rutgers University, Piscataway, New Jersey 08854, United States

ABSTRACT: Protein function depends on both protein structure and amino acid (aa) sequence. Here we show that modular features of both structure and function can be quantified economically from the aa sequences alone for the small (40,42 aa) plaque-forming (aggregative) amyloid beta fragments. Some edge and center features of the fragments are predicted. Bioinformatic scales based on β strand formation propensities and the thermodynamically second order fractal hydropathicity scale based on evolutionary optimization (self-organized criticality) are contrasted with the standard first order physicochemical scale based on complete protein (water−air) unfolding. The results are consistent with previous studies of these physicochemical factors that show that aggregative properties, even of beta fragments, are driven primarily by near-equilibrium hydropathic forces.

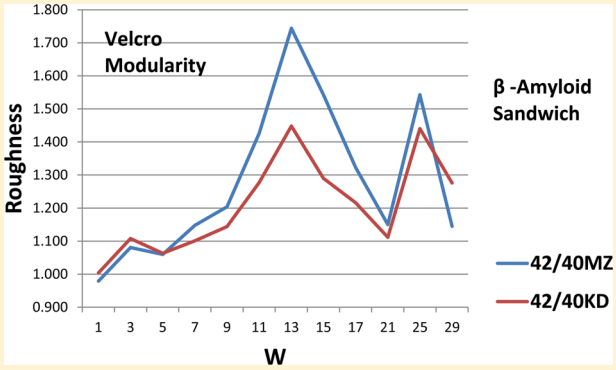

KEYWORDS: *Protein, function, amino acid, sequence, evolutionary, criticality, self-organized*

The amyloid precursor protein APP of Alzheimer's disease (AD) (details available on Uniprot as P05067) has 770 amino acids (aa) and resembles a cell surface receptor. Two small amyloid fragments of A4 (Aβ 40, 672−711 and Aβ 42, 672−713) form plaques. Monomer fragments aggregate to form successive oligomeric globules, proto-fibers, or fibers, with the latter being most toxic. An NMR structural model[1] shows that the cores of these fragments are dominated by a β sandwich structure with halves, β1 = 18−26 and β2 = 31−40 or 31−42, connected by a β turn stabilized by an (E22,D23)-K28 double salt bridge. A hydrophilic loop 1−17 connects successive monomers (Figure 1, from ref 1).

Presently evidence suggests that oligomer intermediates, which lead to fibril formation, may be the primary culprits leading to neuronal dysfunction and cell death.[2] Numerous studies have suggested[3−10] that Aβ 42 is more toxic than Aβ 40. The molecular origin of the biological differences between Aβ 40 and 42 is still under study.[2,11]

Here we examine nonlocal hydropathic Aβ 40 and 42 interactions within a modular framework in which ability to identify both the length scale of the β sandwich structure (Figure 1) and describe the biological differences between Aβ 40 and 42 is used to evaluate the relative importance of different physicochemical factors in describing protein aggregation. Before the bioinformatic scales used here were available, the aggregative properties of lysozyme *c* and acylphosphatase had been previously studied using single amino acid mutagenesis. Distinct chemical factors influence protein properties, and one of the easier general properties to study is aggregation. Reference 12 showed for these two proteins, which are nearly centrosymmetric with respect to their α/β structures, that mutated aggregation rates depend on two leading properties: hydropathicity, and the difference between α helicity and β strand propensities. The first two factors were estimated from empirical aa enthalpy-transfer tables, and it was concluded that globular hydropathic compaction dominates secondary α/β propensities. Is this conclusion still true for the strikingly pure β sandwich structure (Figure 1)?

In earlier papers,[13−17] we discussed the thermodynamic significance of the standard (15 000+ citations) water−air, first-order, enthalpy-based KD hydropathicity scale.[18] The new MZ hydropathicity scale, based on self-organized criticality (SOC), was derived bioinformatically from the differential solvent-exposed geometry of >5000 protein segments.[19] Its derivation strongly suggests second-order character, suitable for describing modular conformational activity, which should dominate most protein functionality. Earlier results from correlations between evolutionary trends in functionalities and aa sequences generally showed better agreement using the MZ scale compared to the KD scale. The evolution of lysozyme *c*, from zebrafish through chickens and mammals to humans, is especially instructive, for its centrosymmetric separation of modular structures into α helix and β strand domains.[14] Mutations in lysozyme *c* are associated with amyloidosis.[14]

Recently bioinformatic scales of α helicity and β strand propensities, separated into different values for exposed and buried residues, have appeared, based again on surveys of

Received: August 12, 2014
Revised: February 17, 2015
Published: February 22, 2015

DOI: 10.1021/cn5001793
ACS Chem. Neurosci. 2015, 6, 745−750

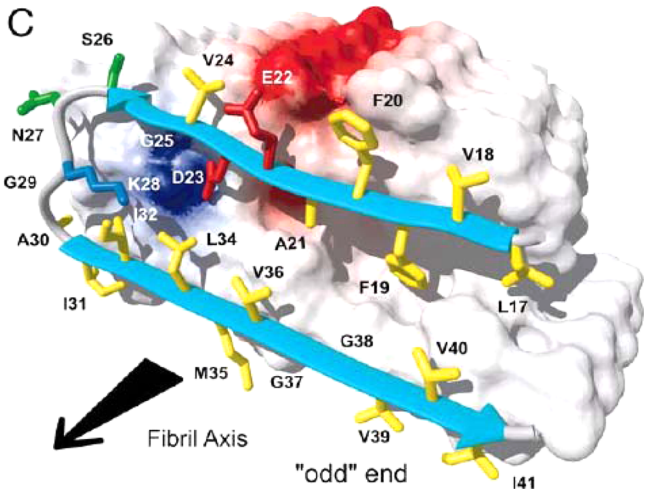

Figure 1. van der Waals contact surface polarity and ribbon diagram of the 17−42 residues of Aβ (Reproduced from Figure 4 of ref 1. Volumes 90−105 (1993−2008) copyright © by the National Academy of Sciences). The 13-mer modular sandwiched β-sheets are indicated by cyan arrows, and the hydrophobic amino acid side chains are shown in yellow. Positively and negatively charged surface patches are shown in blue and red, respectively, with the D23-K28 (E22) salt bridge. The N terminal hydrophilic loop 1−16 (672−687), which connects successive fibrillar molecules, is disordered and is not resolved by NMR solution data.

thousands of PDB structures.[20] Can these propensity scales recognize the 13-mer sandwich structure (Figure 1)?

Earlier work comparing the two ψ(aa,1) hydropathicity scales often examined the variance (or roughness) $\mathcal{R}$ of modular sequences ψ(aa,W), where ψ(aa,W) is ψ(aa,1) averaged over a sliding window of width $W = 2N + 1$:

$$\psi(n, W) = \text{average}[\psi(n - N), \psi(n + N)]$$

$$\mathcal{R}(W) = \text{average}[\psi(n, W) - \text{average}[\psi(n, W)]]^2$$

The intuitive interpretation of W is that it represents the length of a modular element that dominates the protein functionality. The nature of this modular element is especially clear for the amyloid precursor protein A4, whose critical step is fragmentation into Aβ 40 or Aβ 42, here often renumbered as 1−40 or 1−42, respectively. We were able to identify a thermodynamic spinodal, analogous to (P,V) spinodals of elementary van der Waals (vdW) gas−liquid phase diagrams, by identifying two closely spaced weak breaks in slope of the KD $\mathcal{R}(\psi(\text{aa},W))$, and two widely spaced larger breaks in slope of the MZ $\mathcal{R}(\psi(\text{aa},W))$. This shows that the MZ scale corresponds to a lower effective temperature than the KD scale. It explains why the MZ scale gave better correlations between evolutionary trends in functionalities and aa sequences than the KD scale for many other proteins.[21]

Given the A4 spinodal, we also saw that the modular width W is analogous to the molar volume V_m, and $\mathcal{R}$ is analogous to the pressure p in gas−liquid equations of state, such as the vdW equation. Modularity emerges spontaneously in aa distributions of primitive proteins.[22] One can recognize multiple pairwise hydropathicity correlations statistically.[23] Here we have shown that very detailed properties for a given protein can be identified using thermodynamic variables W and $\mathcal{R}$ derived from aa using hydropathic scales.

RESULTS AND DISCUSSION

The amyloid fragments Aβ occur in the 40 aa left half of the compound C-terminal hydrophobic peak.[21] This 80 aa peak is strongly hydrophobic, and rises well above the profile of the rest of A4. It is also about four times as long as a typical 20 aa transmembrane segment of a GPCR protein.[15] It splits in half to form the 40aa Aβ including β1 = 18−26 and β2 = 31−40 or 31−42 fragments, which then self-organize into plaque. One can also connect the 40 aa C-terminal half peak width to the 42aa width of the spinodal tie line between $W = 19$ and $W = 61$ in the log−log plot of $\mathcal{R}(W)$ for A4, Figure 2.[21]

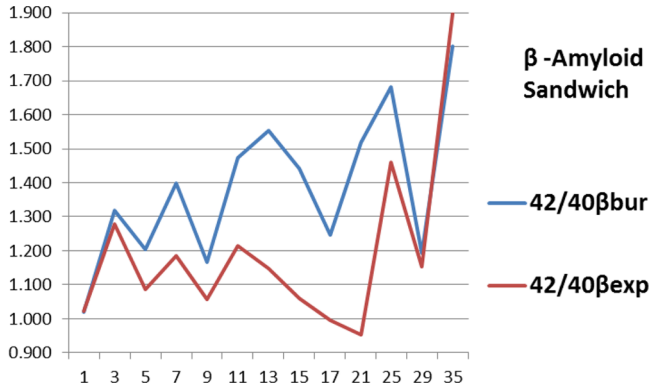

Figure 2. Roughness or variance $\mathcal{R}(W) = \langle\langle\psi(\text{aa},W)\rangle^2\rangle - \langle\langle\psi(\text{aa},W)\rangle\rangle^2$ of amyloid β fragments as a function of the sliding window length W. Because Aβ 40 is much less toxic (aggregative) than Aβ 42, $\mathcal{R}(W)$ of the latter is normalized by $\mathcal{R}(W)$ of the former. There is complex structure in the buried residue β strand plot that can be interpreted as primarily 13- and 26-mers, but the overall β strand profile is noisy.

In Figure 2, we show the roughness ratios $\mathcal{R}_{42}(W)/\mathcal{R}_{40}(W)$ for two kinds of β strand propensities, exposed and buried. The buried profile shows complex structure, which is suggestive of the sandwich structure of Figure 1, but is not so easily interpreted. By contrast, Figure 3 shows the same ratios using the traditional enthalpy transfer scale KD[18] and the modern differential surface area scale MZ.[19] The improvement between Figures 2 and 3 is dramatic, and it scarcely can be explained as either accidental or artificial, as $\mathcal{R}(W)$ has been used often by us for other proteins.[13−15,17]

It is indeed remarkable that such a strikingly simple scaling pattern, resembling diffraction, can result from hydropathic scales alone. As shown in Figure 2, hydropathic modularity is unambiguous, with peaks at $W = W_{max} = 13$, and harmonics at $W = 27$, with both MZ and KD scales. It is striking that the differential MZ scale based on SOC (second-order phase transition) is twice as effective as the complete unfolding (first-order) KD scale in identifying W_{max}. This confirms previous results for the MZ superiority found in other larger proteins.[13−15,17] It is easy to see that W_{max} should be 13, as this divides Aβ into three nearly equal parts, the hydrophilic loop, and the two hydrophobic β_1−β_2 strands. While there may be hundreds of hydropathic scales, this test can be applied to any hydropathic scale, however defined. The superiority of the MZ scale is expected to persist, because it is based on a bioinformatic survey of >5000 protein segments,[19] but the present results can be easily falsified by improving them with some other scale, a task which lies outside the scope of this discussion.

DOI: 10.1021/cn5001793
ACS Chem. Neurosci. 2015, 6, 745−750

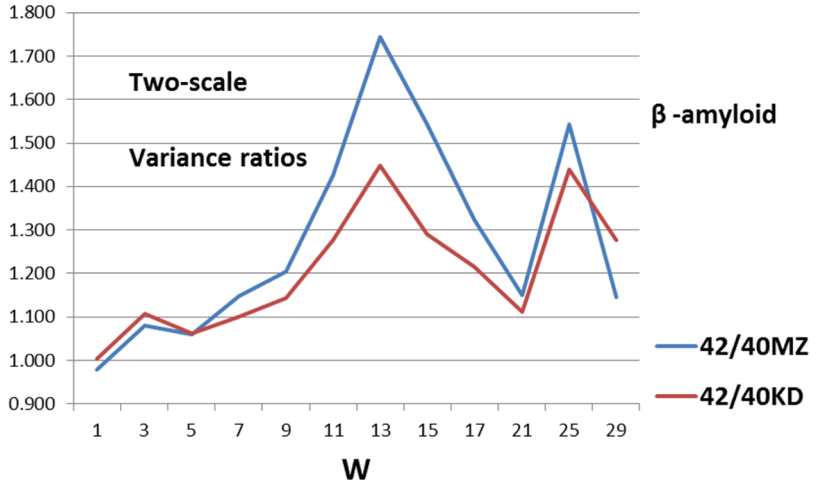

Figure 3. Roughness or variance $\mathcal{R}(W) = \langle\langle\psi(\mathrm{aa},W)\rangle^2\rangle - \langle\langle\psi(\mathrm{aa},W)\rangle\rangle^2$ of amyloid β fragments as a function of the sliding window length W. Because Aβ 40 is much less toxic (aggregative) than Aβ 42, $\mathcal{R}(W)$ of the latter is normalized by $\mathcal{R}(W)$ of the former. Note that simply comparing the values of $\mathcal{R}(1)$ fails, and that the strongest $W = 13$ modularity peak of the sandwiched β-sheets is resolved well even with the KD scale. The MZ scale resolves the modular structure much better than the β strand propensity scale in Figure 1. It also produces a strongest peak that is almost twice as large when W is tuned to 13.

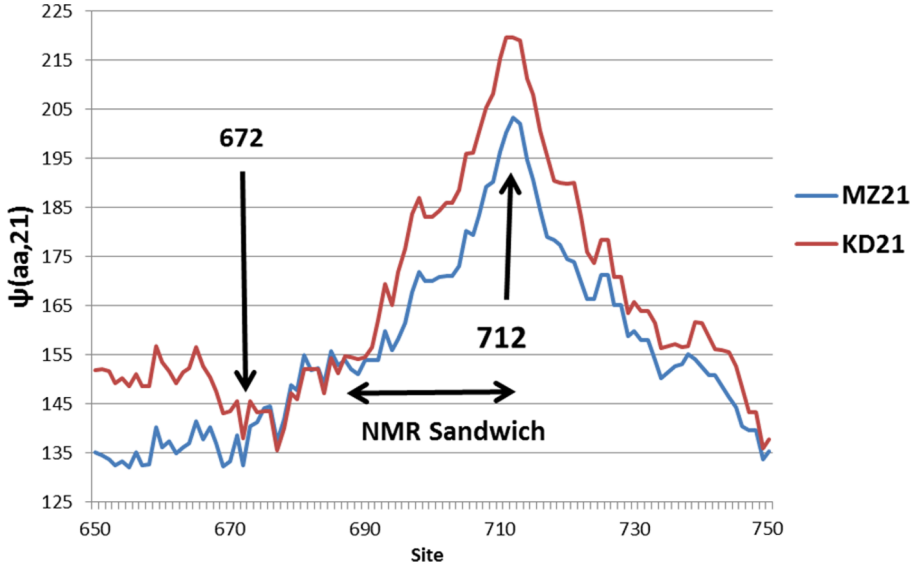

Figure 4. Detail of the wide A4 hydrophobic peak of $\psi(\mathrm{aa},21)$. The beginnings of the amyloid fragments occur just at the hydrophilic cleavage dip at Asp672, and end at the hydrophobic peak 712 ± 1. The flat top of KD21 spans 711−713. It may therefore be said that the KD scale correctly identifies the first-order separation of Aβ40 from Aβ42 (the splitting of 712 ± 1). It is possible that the 3 aa width of this KD flat peak is accurate because fragmentation occurs at a high effective temperature.[17] The range covered by the NMR sandwich model of Figure 1 matches the abrupt increases of the MZ and KD $\psi(\mathrm{aa},21)$ profiles near site 688.

The detailed KD and MZ $W = 21$ profiles show how this connection occurs at the 672 beginning of the hydrophilic loop (Figure 4). As noted in ref 21, $W = W_c = 21$ is a natural choice for the modular W in the vdW equation of state, but it is especially suited to describing A4 fragmentation between 671 and 672 by the membrane-bound enzyme secretase family.[24] Both scales show that the Aβ fragments are strongly amphiphilic,[25] with the left end located at a hydrophilic minimum for $W = 21$, and the right end at a hydrophobic maximum.

The MZ success achieved with $W = 21$ in predicting the 672 and 712 ± 1 cleavage sites is unique. Figure 5 shows the results with other choices of modular length W. These yield extrema near, but not at, the experimental cleavage sites. Profile extrema drift due to numerical noise is natural in such complex proteins, which suggests that the successes achieved with $W = 21$, and particularly the MZ scale, is thermodynamic in nature and derives from the lower effective temperature associated with the MZ scale.

The variance or roughness $\mathcal{R}(W) = \langle[\psi(\mathrm{aa},W)]^2\rangle - [\langle\psi(\mathrm{aa},W)\rangle]^2$ measures the effective pressure p exerted by the "ball bearing" roughness of the protein's water package as it slides and/or tumbles into successive conformations. A simple macroscopic model for the hydrophobic β sandwich shown in Figure 1 supposes that the β1 and β2 strands are stabilized both by the β turn and by mechanical velcrolike roughness of intra- and intersandwich packing under the influence of water pressure. In other words, the larger the roughness, the greater the sandwich, oligomer, and fibril thermal stabilization. This

DOI: 10.1021/cn5001793
ACS Chem. Neurosci. 2015, 6, 745−750

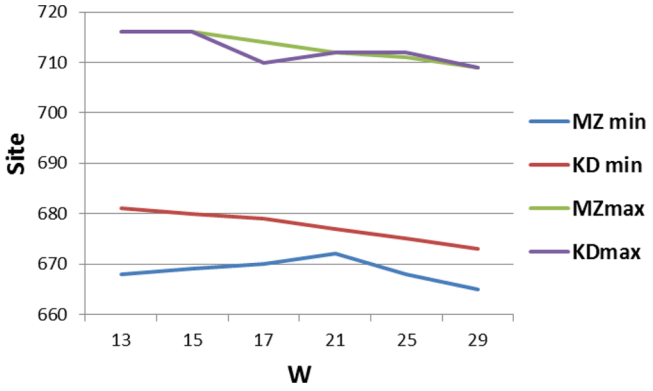

Figure 5. Amphiphilic extrema of ψ(aa,W) profiles in the Aβ range. Figure 2 showed the ψ(aa,21) profiles. This figure shows that the 672 "disordered" cleavage site is predicted correctly by hydrophilic maxima only with the MZ scale and W = 21. The 712 ± 1 cleavage site is predicted correctly by hydrophobic maxima with the KD scale for W = 21 and 25, and with the MZ scale for W = 21.

also explains the remarkable success of the MZ scale in Figure 3.

The differences between the KD complete unfolding scale, and the MZ differential or conformational scale, are neither accidental nor incidental. The associated profiles of ψ(aa,13) are shown in Figure 6. The MZ scale reflects the differences between the hydrophilic loop (1−17) and the hydropathic sandwich strands 18−42 more accurately, which in turn more accurately resolves the modular structure functionality, including even softer hydrophilicity for the hairpin turn, with the MZ scale. Similar plots for W = 9 and W = 17 (not shown) are less informative, as expected from Figure 3.

In discussing A4 (770 aa), we used spinodal breaks to argue[21] that the MZ scale measures fragmentation at a lower effective temperature. One can still define effective temperatures for the Aβ 40/42 fragments from the values of $\mathcal{R}(W)$ for the two scales. This gives effective temperature or $\mathcal{R}(W)$ ratios of KD/MZ ranging from 1.67 (W = 13) to 1.93 (W = 21). These $\mathcal{R}(W)$ ratios are sensible for two reasons: (1) the effective temperatures of the KD scale are higher than those for the MZ scale, and (2) fragmentation is best described by W = 21, where the $\mathcal{R}(W)$ ratio is larger and the effective temperatures are higher, and sandwich reconstruction and aggregation is best described by W = 13 (Figure 3), where the $\mathcal{R}(W)$ ratio is smaller and the effective temperatures are lower.

There are many Aβ familial mutations, and even in vitro these exhibit a wide range of oligomer and fibrous morphologies.[1] Some of these can be explained by roughness changes, with success similar to that achieved by other means, including atomic force microscopy and molecular dynamics. The A673T mutation that reduces β cleavage[26] broadens the hydrophilic minimum centered on Asp 672 (Figure 4), which could explain reduced effectiveness of secretase cleavage.

Our analysis of the β fragments, which are only ∼40 aa long, has confirmed the central conclusion of our earlier thermodynamic analysis[21] of A4 (770 aa). Simple algebraic analysis, using only amino acid sequences, has revealed thermodynamically significant aspects of plaque formation, and distinguished essential features of small (40,42 aa) plaque-forming amyloid β fragments. In the present case, an amphiphilic velcro model has emerged for the β amyloid fragments that may encompass some other β strand structures as well. The amphiphilic features[27] that distinguish the weak β1 = 18−26 and strong β2 = 31−40 or 31−42 hydrophobic β-sheet surfaces on the thermodynamics and kinetics of the polymerization process[28] are quantified. We have also found consistent values of effective temperatures, which are frequently used to describe the thermodynamic properties of glasses and deeply supercooled liquids.[28,29] We have also utilized the full power of bioinformatic methods to test independently the central conclusion of many earlier papers (such as ref 12), that aggregative properties are driven mainly by hydropathic forces, and not secondary structures, here even for pure β sandwiches.

More generally, large-scale structure is recognizable as modules in the community structures of both biological and nonbiological networks that are self-organized.[30] The present thermodynamic method utilizes protein sequence evolution and recognizes modular structures without detailed knowledge of protein folding,[31] and thus provides a remarkably effective and economical tool for connecting sequences to function. The example of amyloid sandwich fragments is a successful functional illustration of protein fractal symmetry.[32] It also shows that the fractal scale is most suitable for irreversible large-scale protein aggregation as well as equilibrium properties, such as describing cytoskeletal actin networks in motile cells as critically self-organized systems.[33]

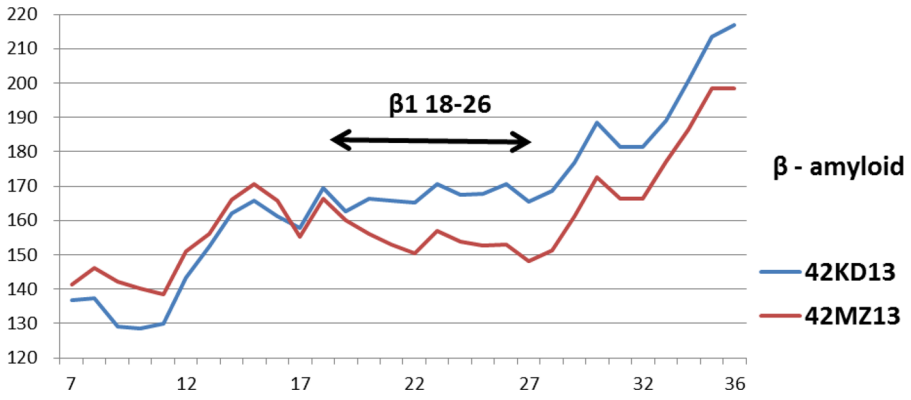

Figure 6. Profiles of ψ(aa,13) for Aβ42 for the MZ SOC differential scale and the first-order KD scale, renumbered with 672 = 1. Note the hydrophilic softening of β_1 at the hairpin turn (26−30, see Figure 1) with the SOC MZ scale. This β_1 softening facilitates formation of the modular sandwich structure, by making its central region more flexible. At the hairpin turn, the W = 13 profile with the KD scale is nearly flat, but there is a local soft hydrophilic minimum promoting a mechanical hinge in the MZ profile at 27.

DOI: 10.1021/cn5001793
ACS Chem. Neurosci. 2015, 6, 745−750

Proteolytic cleavage of APP is driven mainly by more than 150 presenilin mutations. Some time ago, researchers were puzzled by the fact that experimentally reduction of the cleavage rate with fewer mutations increases the concentration ratio of Aβ42/Aβ40; conventionally, this is described as "loss of function".[34] This mystery is resolved by Figure 3. Fewer mutations slow the cleavage rate and bring one closer to equilibrium, and in equilibrium the natural fragment is Aβ 42. Various solutions to this mystery were proposed, including elaborate multichannel, multistage cleavages. The present model (Figure 3) shows (without elaborate mechanisms) that this mysterious effect is merely the result of kinetics near thermodynamic equilibrium.

METHODS

The MZ and KD scaling parameters are tabulated in ref 13. The calculations were made using an EXCEL macro written by Niels Voohoeve and refined by Douglass C. Allan.

AUTHOR INFORMATION

Notes

The authors declare no competing financial interest.

REFERENCES

(1) Luhrs, T., Ritter, C., Adrian, M., Riek-Loher, D., Bohrmann, B., Doeli, H., Schubert, D., and Riek, R. (2005) 3D structure of Alzheimer's amyloid-beta(1−42) fibrils. *Proc. Natl. Acad. Sci. U. S. A. 102*, 17342−17347.

(2) Lotz, G. P., Gregor, P., and Legleiter, J. (2013) The role of amyloidogenic protein oligomerization in neurodegenerative disease. *J. Mol. Med. 91*, 653−664.

(3) Bernstein, S. L., Dupuis, N. F., Lazo, N. D., Wyttenbach, T., Condron, M. M., Bitan, G., Teplow, D. B., Shea, J. E., Ruotolo, B. T., Robinson, C. V., and Bowers, M. T. (2009) Amyloid-beta protein oligomerization and the importance of tetramers and dodecamers in the aetiology of Alzheimer's disease. *Nat. Chem. 1*, 326−331.

(4) Sandberg, A., Luheshi, L. M., Sollvander, S., de Barros, T. P., Macao, B., Knowles, T. P. J., Biverstal, H., Lendel, C., Ekholm-Petterson, F., Dubnovitsky, A., Lannfelt, L., Dobson, C. M., and Hard, T. (2010) Stabilization of neurotoxic Alzheimer amyloid-beta oligomers by protein engineering. *Proc. Natl. Acad. Sci. U. S. A. 107*, 15595−15600.

(5) Murakami, K., Irie, K., Morimoto, A., Ohigashi, H., Shindo, M., Nagao, M., Shimizu, T., and Shirasawa, T. (2003) Neurotoxicity and physicochemical properties of A beta mutant peptides from cerebral amyloid angiopathy - Implication for the pathogenesis of cerebral amyloid angiopathy and Alzheimer's disease. *J. Biol. Chem. 278*, 46179−46187.

(6) Gessel, M. M., Bernstein, S., Kemper, M., Teplow, D. B., and Bowers, M. T. (2012) Familial Alzheimer's Disease Mutations Differentially Alter Amyloid beta-Protein Oligomerization. *ACS Chem. Neurosci. 3*, 909−918.

(7) Fisher, C. K., Ullman, O., and Stultz, C. M. (2013) Comparative Studies of Disordered Proteins with Similar Sequences: Application to Aβ 40 and Aβ 42. *Biophys. J. 104*, 1546−1555.

(8) Dolev, I., Fogel, H., Milshtein, H., Berdichevsky, V., Lipstein, N., Brose, N., Gazit, N., and Slutsky, I. (2013) Spike bursts increase amyloid-beta 40/42 ratio by inducing a presenilin-1 conformational change. *Nat. Neurosci. 16*, 587−+.

(9) Chong, S.-H, Yim, J., and Ham, S. (2013) Structural heterogeneity in familial Alzheimer's disease mutants of amyloid-beta peptides. *Mol. BioSyst.*, 997−1003.

(10) Gu, L., and Guo, Z. F. (2013) Alzheimer's A42 and A40 peptides form interlaced amyloid fibrils. *J. Neurochem. 126*, 305−311.

(11) Lovas, S., Zhang, Y., Yu, J., and Lyubchenko, Y. L. (2013) Molecular Mechanism of Misfolding and Aggregation of A beta(13−23). *J. Phys. Chem. B 117*, 6175−6186.

(12) Chiti, F., Stefani, M., Taddei, N., et al. (2003) Rationalization of the effects of mutations on peptide and protein aggregation rates. *Nature 424*, 805−808.

(13) Phillips, J. C. (2009) Scaling and self-organized criticality in proteins: Lysozyme *c*. *Phys. Rev. E 80*, 051916.

(14) Phillips, J. C. (2014) Fractals and self-organized criticality in proteins. *Phys. A 415*, 440−448.

(15) Phillips, J. C. (2013) Self-Organized Criticality in Proteins: Hydropathic Roughening Profiles of G-Protein Coupled Receptors. *Phys. Rev. E 87*, 032709.

(16) Katritch, V., Cherezov, V., and Stevens, R. C. (2012) Diversity and modularity of G protein-coupled receptor structures. *Trends Pharm. Sci. 33*, 17−27.

(17) Phillips, J. C. (2014) Punctuated evolution of influenza virus neuraminidase (A/H1N1) under opposing migration and vaccination pressures. *BioMed Res. Int.*, 907381.

(18) Kyte, J., and Doolittle, R. F. (1982) A simple method for displaying the hydropathic character of a protein. *J. Mol. Biol. 157*, 105−132.

(19) Moret, M. A., and Zebende, G. F. (2007) Amino acid hydrophobicity and accessible surface area. *Phys. Rev. E 75*, 011920.

(20) Fujiwara, K., Toda, H., and Ikeguchi, M. (2012) Dependence of alpha-helical and beta-strand amino acid propensities on the overall protein fold type. *BMC Struct. Biol. 12*, 18.

(21) PhillipsJ. C. (2013) A cubic equation of state for amyloid plaque formation. arXiv.org e-Print archive. http://arxiv.org/abs/1308.5718.

(22) He, J., Sun, J., and Deem, M. W. (2009) Spontaneous emergence of modularity in a model of evolving individuals and in real networks. *Phys. Rev. E 79*, 031907.

(23) Chou, K. C. (2005) Using amphiphilic pseudo amino acid composition to predict enzyme subfamily classes. *Bioinformatics 21*, 10−19.

(24) Vassar, R., Bennett, B. D., Babu-Khan, S., Kahn, S., Mendiaz, E. A., Denis, P., Teplow, D. B., Ross, S., Amarante, P., Loeloff, R., Luo, Y., Fisher, S., Fuller, L., Edenson, S., Lile, J., Jarosinski, M. A., Biere, A. L., Curran, E., Burgess, T., Louis, J. C., Collins, F., Treanor, J., and Rogers, G. (1999) M. Citron beta-secretase cleavage of Alzheimer's amyloid precursor protein by the transmembrane aspartic protease BACE. *Science 286*, 735−741.

(25) Schubert, D., Behl, C., Lesley, R., Brack, A., Dargusch, R., Sagara, Y., and Kimura, H. (1995) Amyloid peptides are toxic via a common oxidative mechanism. *Proc. Natl. Acad. Sci. U. S. A. 92*, 1989−1993.

(26) Jonsson, T., Atwal, J. K., Steinberg, S., Snaedal, J., Jonsson, P. V., Bjornsson, S., Stefansson, H., Sulem, P., Gudbjartsson, D., Maloney, J., Hoyte, K., Gustafson, A., Liu, Y. C., Lu, Y. M., Bhangale, T., Graham, R. R., Huttenlocher, J., Bjornsdottir, G., Andreassen, O. A., Jonsson, E. G., Palotie, A., Behrens, T. W., Magnusson, O. T., Kong, A., Thorsteinsdottir, U., Watts, R. J., and Stefansson, K. (2012) A mutation in APP protects against Alzheimer's disease and age-related cognitive decline. *Nature 488*, 796−99.

(27) Auer, S. (2014) Amyloid fibril nucleation: effect of amino acid hydrophobicity. *J. Phys. Chem. B 118*, 5289−5299.

(28) Cugliandolo, L. F., Kurchan, J., and Peliti, L. (1997) Energy flow, partial equilibration, and effective temperatures in systems with slow dynamics. *Phys. Rev. E 55*, 3898−3914.

(29) Berthier, L., and Barrat, J. L. (2002) Shearing a glassy material: Numerical tests of nonequilibrium mode-coupling approaches and experimental proposals. *Phys. Rev. Lett. 89*, 095702.

(30) Newman, M. E. J. (2012) Communities, modules and large-scale structure in networks. *Nat. Phys. 8*, 25−31.

(31) Sali, A., Shaknovich, E., and Karplus, M. (1994) How does a protein fold. *Nature 369*, 248−251.

(32) Banerji, A., and Ghosh, I. (2011) Fractal symmetry of protein interior: what have we learned? Cell. Mol. *Life Sci. 68*, 2711−2737.

(33) Cardamone, L., Laio, A., Torre, V., Shahapure, R., and DeSimone, A. (2011) Cytoskeletal actin networks in motile cells are critically self-organized systems synchronized by mechanical interactions. *Proc. Natl. Acad. Sci. U. S. A. 108*, 13978−13983.

DOI: 10.1021/cn5001793
ACS Chem. Neurosci. 2015, 6, 745−750

(34) Wolfe, M. S. (2007) When loss is gain: Reduced presenilin proteolytic function leads to increased Abeta42/Abeta40. Talking Point on the role of presenilin mutations in Alzheimer disease. *EMBO Rep. 8*, 136−140.

DOI: 10.1021/cn5001793
ACS Chem. Neurosci. 2015, 6, 745−750